

Vector-Mode Decay in Atmospheric Turbulence: An Analysis Inspired by Quantum Mechanics

Isaac Nape¹, Nikiwe Mashaba^{1,2}, Nokwazi Mphuthi¹, Sruthy Jayakumar³, Shanti Bhattacharya³, and Andrew Forbes^{1,*}

¹*School of Physics, University of the Witwatersrand, Private Bag 3, Johannesburg 2050, South Africa*

²*Optronic Sensor Systems, Defence and Security, Council for Scientific and Industrial Research (CSIR), Pretoria 0001, South Africa*

³*Department of Electrical Engineering, Indian Institute of Technology Madras, Chennai 600036, India*



(Received 29 November 2020; revised 12 January 2021; accepted 29 January 2021; published 10 March 2021)

Vector beams are inhomogeneously polarized optical fields with nonseparable quantumlike correlations between their polarization and spatial components, and they hold tremendous promise for classical and quantum communication across various channels, e.g., the atmosphere, underwater, and in optical fiber. Here, we show that by exploiting their quantumlike features by virtue of the nonseparability of the field, the decay of both the polarization and spatial components can be studied in tandem. In particular, we invoke the principle of channel-state duality to show that the degree of nonseparability of any vector mode is purely determined by that of a maximally nonseparable one, which we confirm using orbital angular momentum (OAM) as an example for topological charges of $\ell = 1$ and $\ell = 10$ in a turbulent atmosphere. A consequence is that the well-known cylindrical vector vortex beams are sufficient to predict the behavior of all vector OAM states through the channel. Our method reveals interesting features about the performance of various modes through the channel: the decay in vector quality decreases with an increasing OAM value, even though the spread is higher for larger OAM modes. Our approach offers a fast and easy probe of noisy channels, while at the same time revealing the power of quantum tools applied to classical light.

DOI: 10.1103/PhysRevApplied.15.034030

I. INTRODUCTION

Structured light has become topical of late [1], with so-called cylindrical-vector-vortex (CVV) beams [2] taking center stage in numerous fundamental and applied studies [3,4]. For example, they form a family of natural solutions of free-space and optical waveguides and have been used in optical trapping [5–7] and metrology [8], as well as high-capacity classical [9–11] and quantum [12–15] communication. To meet the demand of such growing applications, a plethora of generation methods have emerged, including directly from lasers [16–18], or externally with liquid crystal q -plate technology [19], metasurfaces [20,21], and spatial light modulators [22]. Detection has likewise matured to include deterministic detectors incorporating interferometers [23,24], mode sorters, [25] or both [26], as well as fast digital Stokes measurements [27–29] and direct measures of the nonseparability or vector quality factor [30,31], giving a quantitative measure of how “vector” the vector beam is.

An open challenge in the context of classical and quantum communication is the propagation of such modes

through media exhibiting spatially dependent perturbations. These might include thermal effects due to overheating of optical elements [32], rapid refractive-index fluctuations in the atmosphere [33,34] and underwater [35], and in optical fiber [36,37]. In particular, atmospheric turbulence leaves the polarization of optical beams undisturbed while the spatial components degrade rapidly, resulting in modal scattering and therefore information loss [38–45]. Consequently, information encoding with the spatial components of light is restricted to only several kilometers [46,47]. In the case of vector beams having coupled polarization and spatial components, the polarization fields are indirectly impacted [48], resulting in the decay of nonseparability or “vectorness” [49].

Here, we exploit parallels between nonseparability of vector beams and entanglement in quantum systems [49–56] to deploy a quantum toolkit for the study of vector beams in atmospheric turbulence. We recognize that just as the degree of entanglement of any pure quantum state can be determined by that of a maximally entangled state [57], courtesy of the Choi-Jamiołkowski isomorphism (channel-state duality) [58,59], so it must be true that the dynamics of any vector beam in a one-sided noisy channel should be able to be inferred from the dynamics of just one beam, a

*andrew.forbes@wits.ac.za

purely inhomogeneously polarized field (a perfectly “vector” beam with orthogonal spatial modes), which from now on we refer to as ideal vector-vortex (VV) beams. In the context of OAM, any one of the CVV beams with opposite spin and OAM states would suffice, as well as VV beams in the linear polarization basis. Using such beams as a probe, we confirm the Choi-Jamiolkowski isomorphism for classical vectorial light and show that the “vectorness” decay of all initial beams can be predicted from the decay of an ideal VV beam. The approach is first outlined using CVV beams and then generalized to other VV beams for adaptability. We illustrate this for two OAM subspaces, $\ell = \pm 1$ and $\ell = \pm 10$, revealing from this measure a simple factor for the rate at which one subspace decays relative to the other. Our work not only offers a simple tool for probing classical communication channels but also reveals insights into the decay dynamics of vectorial OAM light. While we demonstrate the approach with OAM in the atmosphere, it can easily be adapted to other mode sets and media, and likewise to hybrid entangled quantum states.

II. CONCEPTS

Here, we elucidate the concept of channel-state duality with nonseparable vector beams for characterizing classical beams through perturbing media. We first introduce the key concepts of nonseparability in vector beams, vector-beam decay through turbulence, and then finally channel-state duality. The core idea is that an ideal vector beam is sufficient to predict the behavior of any vector beam, even partially “vector,” through a channel.

A. Nonseparable vector modes

To construct an ideal VV beam, we require a vectorial superposition of spatial mode and polarization where the nonseparability is maximum. We illustrate the concept of nonseparability using familiar CVV beams since they are ubiquitous in a myriad of applications [60]. Thereafter, we extend the concept to a family of VV beams by a simple change of basis in the polarization components.

CVV beams are natural solutions of the vectorial Helmholtz equation in cylindrical coordinates. An example of one such beam, which has a radially symmetric polarization field, is shown in Fig. 1(a). Such beams are commonly represented as superpositions of scalar fields coupled to orthogonal circular polarization states, i.e.,

$$\Psi_\ell(\mathbf{r}) = a \exp(i\ell\phi) \hat{e}_R + b \exp(-i\alpha) \exp(-i\ell\phi) \hat{e}_L, \quad (1)$$

where $\mathbf{r} = (r, \phi, z = 0)$ are the cylindrical coordinates, $\hat{e}_{R,L}$ are the canonical right and left circular polarization states, respectively. The polarization modes are coupled to spatial modes having characteristic azimuthal phase profiles $\exp(\pm i\ell\phi)$, associated with light fields carrying an OAM of $\pm \ell \hbar$ per photon, respectively. Here, the unbounded

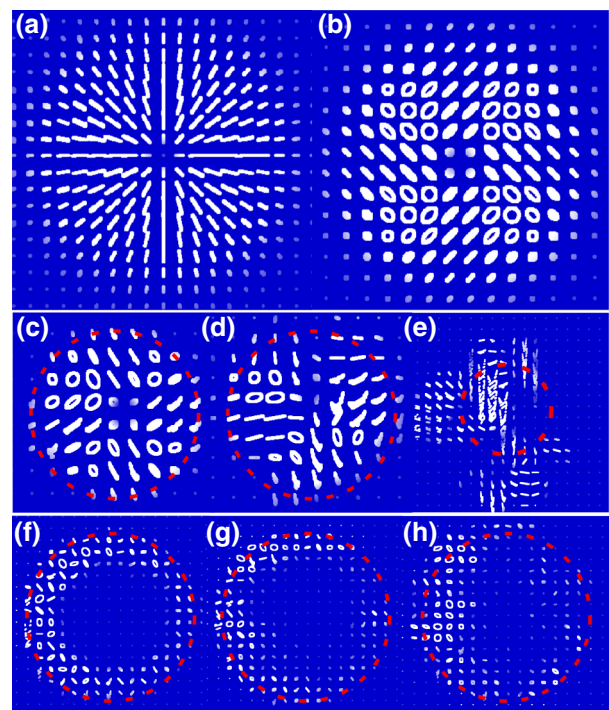


FIG. 1. Example theoretical polarization field profiles of (a) a CVV beam and (b) a VV beam. The CVV beam has nonuniform linear polarization states while the VV beam varies between linear and elliptical polarization states. Both beams have a VQF of 1. Experimental polarization fields of vector modes transmitted through turbulence with varying strengths from left to right, initially encoded in OAM subspaces (c)–(e) $|\ell| = 1$ and (f)–(h) $|\ell| = 10$ in the second and third bottom panels, respectively. The turbulence strengths are $D/r_0 = 0$ (no turbulence), $D/r_0 = 2.5$, and $D/r_0 = 3.5$ in each column, respectively.

integer, $\pm \ell$, is the topological charge. The parameters a , b , and α are the relative amplitudes and phases between the modes in the superposition. Next, we show that the coupling between the polarization and spatial components is reminiscent of quantum entanglement between two particles.

It is common to represent the polarization and spatial components of vector modes as state vectors using the Dirac notation from quantum mechanics, i.e., $\hat{e}_{R(L)} \rightarrow |R(L)\rangle$ and $\exp(\pm i\ell\phi) \rightarrow |\pm \ell\rangle$, enabling a more compact representation of Eq. (1) following

$$|\Psi_\ell\rangle = a|R\rangle + b \exp(-i\alpha)|-\ell\rangle|L\rangle. \quad (2)$$

Here, the bra-ket notation is used to mark the spatial and polarization components, making it convenient to express each degree of freedom (DOF) as a unique subsystem analogous to two particle states in quantum mechanics. By clearly identifying each DOF, we wish to quantify the amount of nonseparability between them. This can be achieved by using the vector quality factor (VQF) [30,31], which is an analogous measure of entanglement based

on the concurrence [61] but between the internal DOF of the classical light fields. For the state in Eq. (2), the VQF, equivalently the concurrence, is therefore given by $VQF = |ab|$ ranging from $VQF = 0$ for a separable scalar beam ($a = 0$ or $b = 0$) to $VQF = 1$ for a nonseparable vector beam ($a = b$); and otherwise partially “vector” for $0 < VQF < 1$. This measure has been used in a myriad of experiments as a witness for nonseparability in classical beams [27,62,63].

Note that in the circular polarization basis, vector beams of varying nonseparability are spanned on a four-dimensional state space and therefore have the general form

$$|\Phi_\ell\rangle = a|\ell\rangle|R\rangle + b|-\ell\rangle|R\rangle + c|\ell\rangle|L\rangle + d|-\ell\rangle|L\rangle, \quad (3)$$

with a corresponding degree of nonseparability

$$VQF = |ad - cb|, \quad (4)$$

assuming that the coefficients satisfy, $(|a|^2 + |b|^2 + |c|^2 + |d|^2) = 1$. One can simply recover the previous vector beam, for example, by setting ($a = b$), while $cb = 0$. This becomes crucial when studying the decay of vector beams, since we always project onto the entire subspace ($\pm\ell$) of spatial modes with which we started.

Next, we show that the coupling between the DOFs of any spatial mode that is transmitted through a complex medium, using turbulence as an example, can be determined by that of a maximally nonseparable vector mode by exploiting channel-state duality.

B. Propagation of vector modes through turbulence and channel-state duality

Structured light is known to be perturbed in atmospheric turbulence [64]. In particular, a vector mode propagating through turbulence experiences phase-dependent fluctuations that have an impact on its transverse spatial components. Assuming weak irradiance fluctuations approximated by Kolmogorov theory [33], the phase variations can be characterized by the phase-structure function, $D_\phi(\mathbf{r}_1, \mathbf{r}_2) = 6.88\Delta r/r_0$, where r_0 is the Fried parameter [65], which describes the transverse scale of the atmospheric distortions and $\Delta r = |\mathbf{r}_1 - \mathbf{r}_2|$ are relative displacements in the transverse plane. For an optical system with a diameter (aperture) D , we can associate the turbulence strength with the normalized aperture size, D/r_0 , relating the turbulence strength to the relative transverse distance within which the refractive index is correlated. For example, a large aperture size *seeing* a smaller Fried parameter ($D > r_0$) experiences more distortions than a smaller aperture *seeing* a larger Fried parameter ($D < r_0$). In this paper, D approximates the size of the beam. We

show examples of the effect of turbulence on the polarization field of vector modes in Figs. 1(c)–1(h). The polarization field as well as the spatial distribution gets deformed with increasing turbulence strength (from left to right). We investigate how the distortions affect the nonseparability.

Now, since the atmosphere is nonbirefringent, only the transverse spatial components of the mode expressed in Eq. (2) are perturbed and as a consequence there is modal scattering into adjacent OAM modes [48]. For example, an OAM mode corresponding to the state $|\ell\rangle$ traversing a medium with the channel matrix $\hat{T} = \sum_{m,n} c_{n,m} |m\rangle\langle n|$, transfers energy from the initial state into its neighboring eigenmodes following the mapping

$$|\ell\rangle \xrightarrow{\hat{T}} \sum_m c_{\ell,m} |m\rangle, \quad (5)$$

where $P(\ell, m) = |c_{\ell,m}|^2$ is the conditional probability for the mode $|\ell\rangle$ to exchange energy with the mode $|m\rangle$. For Kolmogorov turbulence, the probabilities have been determined analytically [66] and are symmetric about $|\ell\rangle$ for weak turbulence.

With this in mind, we can now describe the state of our CVV mode after it traverses the turbulent channel. Let us assume that vector mode is initially in the state

$$|\Psi_\ell\rangle = 1/\sqrt{2} (|\ell\rangle|R\rangle + |-\ell\rangle|L\rangle). \quad (6)$$

Upon traversing the channel, the OAM modes scatter according to Eq. (5). By projecting back onto the initial OAM subspace, i.e., $\{|-\ell\rangle, |\ell\rangle\}$, we obtain the state

$$\begin{aligned} |\tilde{\Psi}_\ell\rangle = \mathcal{N} (&c_{\ell,\ell}|\ell\rangle|R\rangle + c_{\ell,-\ell}|-\ell\rangle|R\rangle + c_{-\ell,\ell}|\ell\rangle|L\rangle \\ &+ c_{-\ell,-\ell}|-\ell\rangle|L\rangle). \end{aligned} \quad (7)$$

Here, \mathcal{N} is a normalization factor, satisfying $|\langle \tilde{\Psi}_\ell | \tilde{\Psi}_\ell \rangle|^2 = 1$. We are assuming that the losses are identical for the spatial modes that make up the vector beam, which is true for our case and indeed all the CVV beams. In this case, the overall losses can be ignored as they play no part in the analysis. The VQF becomes

$$VQF_{\max} = 2|\mathcal{N}|^2 |c_{\ell,-\ell}c_{-\ell,\ell} - c_{\ell,\ell}c_{-\ell,-\ell}|. \quad (8)$$

By applying the notion of the Choi-Jamiołkowski isomorphism (channel-state duality), we hypothesize that any other vector mode with initial “vectorness” of VQF_{in} will decay according to the factorization law

$$VQF_{\text{out}} = VQF_{\max} \times VQF_{\text{in}}, \quad (9)$$

where VQF_{out} is the nonseparability of the state after the channel. In other words, the decay of any arbitrary vector beam can be inferred by simply propagating an ideal

vector beam through the channel to find the scale factor, VQF_{\max} . Rather than propagating many beams through the channel, only one beam has to be passed through to understand its impact. Remarkably, the properties of the channel are determined by its interaction with a maximally nonseparable vector mode. This means that by knowing how a maximally nonseparable vector mode propagates through turbulence, it is possible to predict how the nonseparability of any other arbitrary superposition state evolves. Equation (9) also predicts that the trend is linear and has an intercept at zero, with the decay of the CVV beam returning the slope (VQF_{\max}).

This intriguing property can be understood from the perspective of quantum mechanics. First, the channel weights, $|\langle \pm \ell | \hat{T} | \ell \rangle|^2$, are imprinted on the input nonseparable state mapping the channel onto a pure state, as a consequence of the Choi–Jamiolkowski isomorphism [58,59]. Equivalently, a vector mode traversing a noisy channel has similar properties owing to the nonseparability of the spatial and polarization components. This means that the final VQF of any partial nonseparable mode can be determined by that of a maximally nonseparable vector mode.

Finally, although we have used the CVV beam as a well-known example, in general the polarization and spatial components can be in any basis. For convenience going forward and in the experiment, we will convert to the horizontal ($|H\rangle$) and vertical ($|V\rangle$) polarization basis while the spatial profiles are defined in the Laguerre-Gaussian (LG) basis. As a result, we no longer have a CVV beam, since there is no cylindrical symmetry in the polarization field. An example of our VV beam is shown in Fig. 1(b),

where the polarization states across the transverse plane are mixtures of linear and elliptical states. Such a beam is represented by the state

$$|\Psi_\ell\rangle = a|\ell\rangle|H\rangle + b|-\ell\rangle|V\rangle, \quad (10)$$

with the same $VQF = 1$ as that of Eq. (2). This serves to make it clear than any ideal VV is sufficient for the test.

III. METHODS

A. Experimental setup

We describe the generation and detection scheme illustrated in Fig. 2(a). We use a helium-neon (He-Ne) laser with a central wavelength of 633 nm and a collimated Gaussian field profile. As the approach is not influenced by the wavelength, we select our laser for convenience only. We modulate the laser beam using a phase-only HOLO-EYE PLUTO spatial light modulator (SLM). To obtain the states $|\Psi\rangle_{\ell=1,10}$, we encode the multiplexed holograms [60] with LG modes of charges $\ell = -1(-10)$ and $\ell = 1(10)$ and subsequently separate them in path using a D-shaped mirror. The amplitudes and phases of each mode are encoded using the Arrizon technique for complete amplitude and phase control [67]. An example of one of the holograms is shown in Fig. 2(b).

Before interfering the two beams at the BS, we rotate the polarization of the reflected beam from the D-shaped mirror by 90° using a half-wave plate. This converts the polarization from H to V. The two beams now have orthogonal polarizations. After combining the two beams, the resulting vector mode is transmitted to the digital micromirror

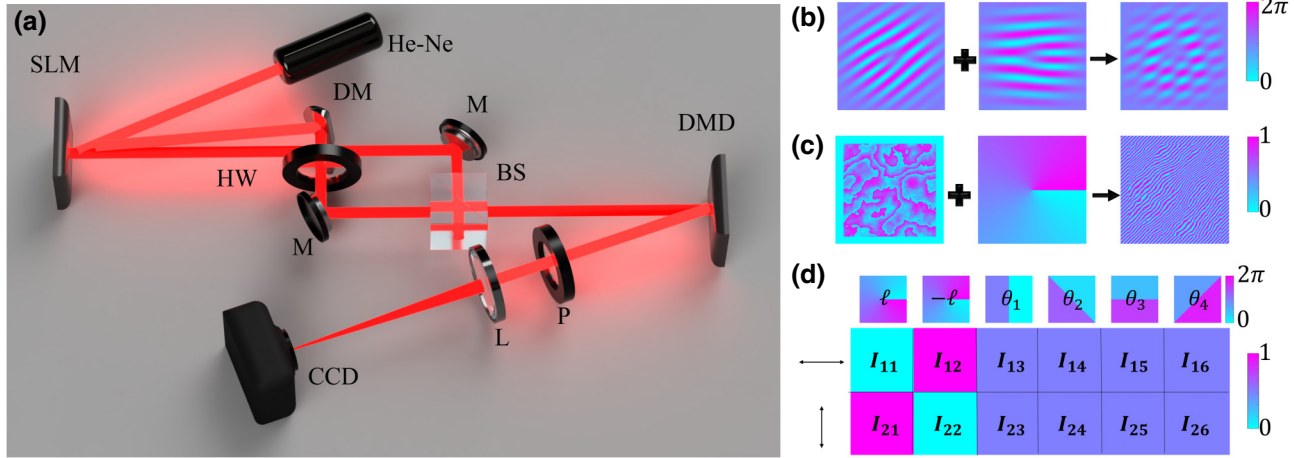


FIG. 2. (a) An illustration of the experimental setup. A helium-neon (He-Ne) laser is expanded and collimated onto a spatial light modulator (SLM). On the SLM, two modes with oppositely charged OAM and distinct gratings frequencies are encoded on a single hologram as shown in (b). Upon propagation, the modes separate in path. Since they propagate closely, a D-shaped mirror (DM) is used to redirect one of them. A half-wave (HW) plate is used to rotate the polarization of the redirected beam. The modes are subsequently recombined at a beam splitter (BS). The resulting mode is imaged to the digital micromirror device (DMD), where (c) turbulence is encoded in combination with the detection holograms. Polarization projections are performed with a linear polarizer (P). Finally, the resulting mode is propagated to the far field with a 500-mm Fourier lens (L), where an on-axis intensity measurement is performed using a CCD camera. (d) An example of the measurements needed to calculate the nonseparability, i.e., the VQF, of the vector modes.

device (DMD). On the DMD, we encode Kolmogorov turbulence phase screens following Ref. [68] in combination with the detection holograms necessary for the VQF measurements. An example of one of the detection holograms is shown in Fig. 2(c) as a combination of the detection mode and the turbulence phase screen, resulting in a noisy detection hologram that has both the perturbation from turbulence and projection mode. The VQF projection holograms, with no turbulence, have phase profiles shown in the first row of Fig. 2(d), shown for the $\ell = \pm 1$ subspace.

Lastly, we use a polarizer to project onto the H and V polarization modes after the DMD. The resulting field is then propagated to the far field using a Fourier lens (L) and an on-axis measurement of the intensity is recorded, providing the modal overlap of the input state, the simulated turbulence, and the detection mode [69]. For each measurement we prepare up to 30 instances of each turbulence strength ranging from $D/r_0 = 0$ to 3.5 in steps of $D/r_0 = 0.5$. An example of measurements for intensities I_{uv} is shown in Fig. 2(d) for a perfect vector mode. The columns correspond to the spatial projections while the rows correspond to the polarization measurements. Next, we show how the VQF (nonseparability) is measured.

B. Vector-quality-factor measurement

We follow the procedure outlined in Ref. [30] to measure the nonseparability of the vector modes. The VQF is given by

$$\text{VQF} = \sqrt{1 - \sum_i^3 \langle \sigma_i \rangle^2}, \quad (11)$$

where the expectation values of the Pauli matrices $\langle \sigma_i \rangle$ can be obtained from

$$\langle \sigma_1 \rangle = I_{13} + I_{23} - (I_{15} + I_{25}), \quad (12)$$

$$\langle \sigma_2 \rangle = I_{14} + I_{24} - (I_{16} + I_{26}), \quad (13)$$

$$\langle \sigma_3 \rangle = I_{11} + I_{21} - (I_{12} + I_{22}). \quad (14)$$

The detection probabilities I_{uv} , $u = \{1, 2\}$, and $v = \{1, 2, \dots, 6\}$ are determined from six identical projections of different polarization-basis states, namely horizontal and vertical polarizations. The projections are performed by inserting a polarizer, set to 0° and 90° for the horizontal and vertical polarization projections, respectively. The six spatial measurements consist of projections onto OAM states $|\pm\ell\rangle$ and their four superpositions $|\theta\rangle = |-\ell\rangle + e^{i\theta/|\ell|}|\ell\rangle$, with $\theta = 0, \pi/2, \pi$, and $3\pi/2$. The spatial projections are encoded as binary holograms onto the digital micromirror device using the method in Ref. [70], tailored for

amplitude-only devices. Finally, the on-axis intensity due to each projection is measured in the focal plane of a Fourier lens using a CCD camera, in the first diffraction order.

IV. RESULTS

A. Propagation of vector modes through turbulence

We first generate vector modes ($|\Psi_\ell\rangle$) and subsequently measure their resulting polarization ellipses and/or fields using Stokes polarimetry. For brevity, see Ref. [29] (Secs. II and V) for calculations of the Stokes parameters and further details on extracting the polarization ellipses. The polarization profiles are shown in Figs. 1(c)–1(h) for $|\Psi_1\rangle$ and $|\Psi_{10}\rangle$, respectively. In each panel, the profiles are shown for increasing turbulence strengths $D = 0, 2.5$ and 3.5 , from left to right. The intensity profile is shown to deteriorate in each instance, confirming the presence of distortions in the transverse plane of the fields.

Next, we measure the modal spectrum of each polarization component averaged over 30 instances of the same turbulence strength. The results are shown in Figs. 3(a)–3(c) for $|\Psi_{\ell=1}\rangle$ and in Figs. 3(d)–3(f) for $|\Psi_{\ell=10}\rangle$. For each ℓ -dependent mode, the turbulence strength is $D/r_0 = 0$ (a,d) $D/r_0 = 2.5$ (b,e) and $D/r_0 = 3.5$ (c,f). In each plot, the distribution on the right corresponds the horizontally polarized mode (blue), while the distribution on the left (red) corresponds to the vertically polarized mode. As expected, the mode distribution is symmetric about $|\ell|$, consistent with the theoretical distribution shown as lines [71]. We measure the width of each distribution as twice the standard deviation, using the formula

$$\Delta\ell = 2\sqrt{\frac{\sum_m |m - \bar{\ell}| P(\ell, m)}{\sum_m P(\ell, m)}}, \quad (15)$$

where $\bar{\ell}$ is the mean OAM in the field. For $D/r_0 = 2.5$, we measure a width of $\Delta\ell = 3.18$ and $\Delta\ell = 6.64$ for $|\Psi_{\ell=1}\rangle$ and $|\Psi_{10}\rangle$, respectively, averaged over both polarization components of the beams. With an increased turbulence strength, $D/r_0 = 3.5$, we measure a width of $\Delta\ell = 4.44$ and $\Delta\ell = 8.79$. In both cases, the OAM width of $\ell = 10$ vector modes is higher than that of $\ell = 1$ vector modes (twice as high), showing that higher-order OAM modes spread farther than lower-order OAM modes, which is consistent with the theory [48].

While this reveals information about how the spatial components are perturbed, we now investigate how the polarization in tandem with the spatial components is affected, testing our isomorphism hypothesis.

To illustrate the effect of the mode scattering on the nonseparability, we show the theoretical (lines) and experimental (points) of VQF values measured for $|\ell| = 1, 10$ subspaces as a function of the turbulence strength in Fig.

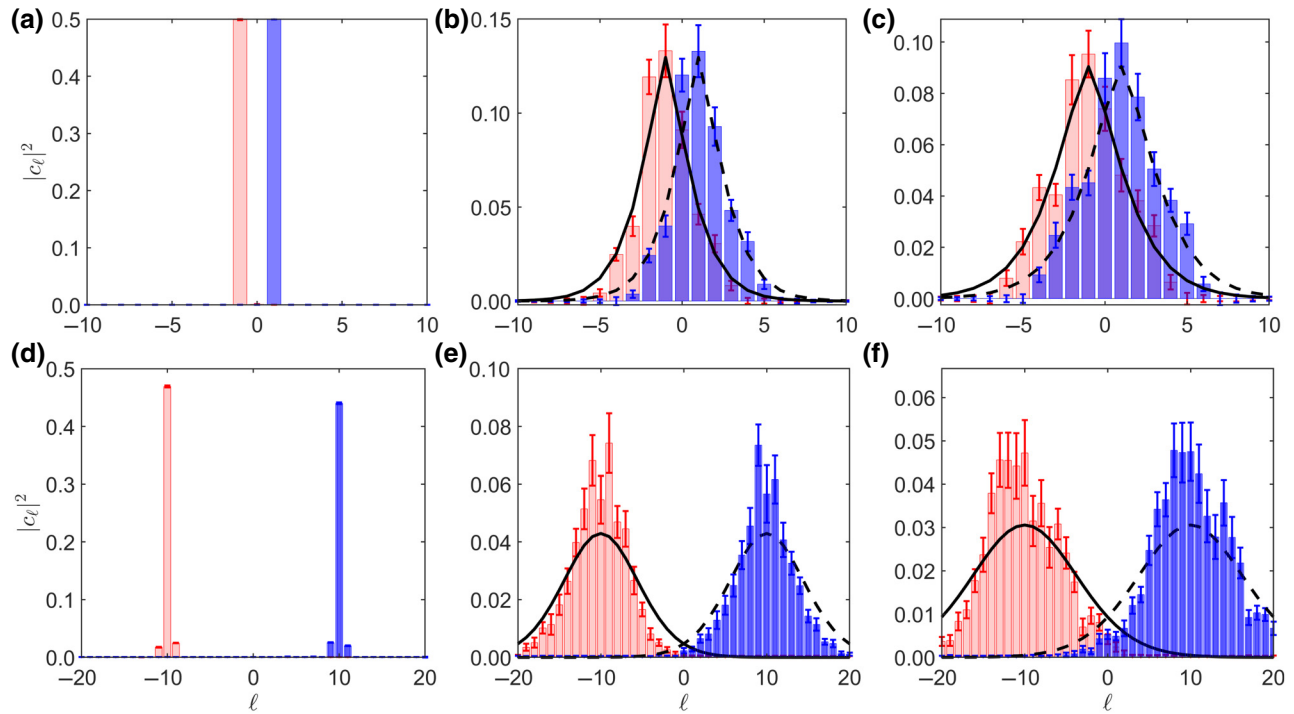


FIG. 3. The measured modal spectrum for the vertical and horizontal polarized components of vector modes in OAM subspaces corresponding to $\ell = 1$ (top panel) and $\ell = 10$ (bottom panel), with (a,d) no turbulence $D/r_0 = 0$ and increased turbulence strengths of (b,e) $D/r_0 = 2.5$ and (c,f) $D/r_0 = 3.5$. The solid lines correspond to the theoretical spectrum. The asymmetry in the mode distributions can be attributed to the statistical fluctuations in the data due to imperfections induced by phase drifts from our interferometer as well as aberrations on the DMD.

4(a). The VQF of the $\ell = 10$ modes decays at a lower rate than the VQF of the $\ell = 1$ modes, analogous to the decay of entangled photons through a single-sided channel of turbulence [39]. This can be explained by the higher mode separation between the spatial components of the generated vector modes; the scattering onto the other modes happens in both cases and it takes longer for larger OAM ($\ell = 10$) to diffuse onto opposite sides than for lower OAM ($\ell = 1$). While the above analysis is performed on input modes with a high nonseparability (VQF ≈ 1), next we evaluate how vector modes with a varying degree of nonseparability also decay under the same turbulence strength. We demonstrate this to confirm the channel-state duality inherent in vector modes propagated through a perturbation channel acting on the spatial DOF. The results are shown in Figs. 4(b) and 4(c) under turbulence conditions of $D/r_o = 2.5$ and 3.5, respectively. This is done for subspaces $\ell = \pm 1$ (circles) and $\ell = \pm 10$ (squares).

The error bars for the x axis are smaller than the points. To control the VQF of the input mode, we adjust the grating depth of the hologram corresponding to the $\ell = -1(-10)$ mode. The plots show that the output VQF, i.e., VQF_{out} , has a linear relation to the input VQF where the line fitted through each data set has a gradient, m_ℓ or, equivalently, VQF_{max} , which is equivalent to the VQF of a

maximally nonseparable vector mode transmitted through the same turbulence. We show the gradient of each line in Table I as well as the goodness of fit, which is above $R^2 = 0.96$. A perfect fit would result in $R^2 = 1$. As shown, the gradients of the $\ell = 10$ modes are higher than those of $\ell = 1$, owing to the higher crosstalk in the $\ell = 1$ subspace, as demonstrated earlier. For $D/r_o = 3.5$, we find that for the $\ell = 10$ subspace, the gradient can be 4 times larger in comparison to the $\ell = 1$ subspace. Since the gradient indicates the maximum VQF that a vector mode with an input nonseparability of $VQF_{\text{in}} \approx 1$ can obtain, after propagating through the channel, all partially nonseparable vector modes within the same subspace are bounded on the interval $VQF_{\text{out}} \in [0, m_\ell]$, consistent with the factorization law [57] for single-sided channels, indicating that vector modes possess the ability to probe the channel-state duality of noisy channels. Indeed, our results show that the decay in nonseparability of any vector mode decays through the medium according to the relation $VQF_{\text{out}} = VQF_{\text{in}} \times m_\ell = VQF_{\text{in}} \times VQF_{\text{max}}$, where $VQF_{\text{max}} = VQF(\hat{T}|\Psi\rangle_\ell)$ is the VQF of a vector mode, $|\Psi\rangle_\ell$, after traversing the channel, \hat{T} , and having an initial VQF of 1, while VQF_{in} is the VQF of the mode we wish to characterize after the channel. The isomorphism implies that one maximally nonseparable vector beam is needed to probe a channel,

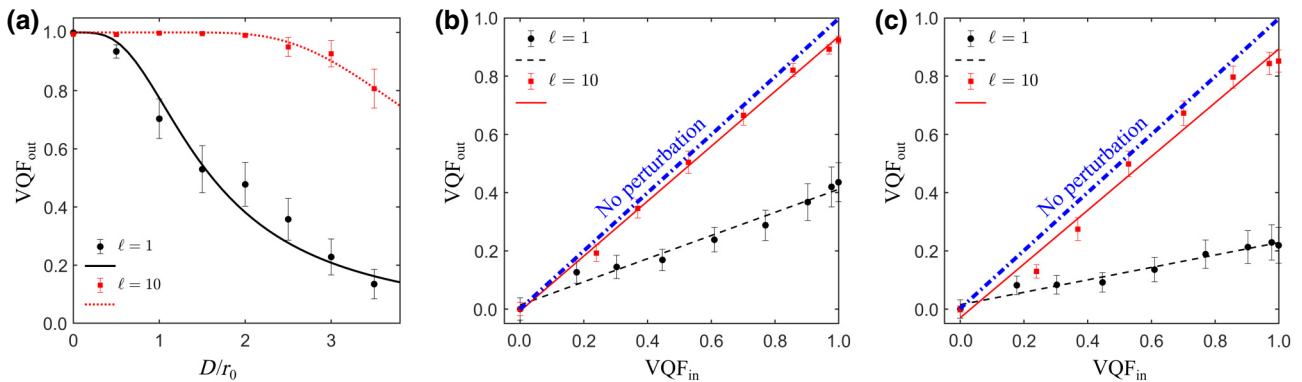


FIG. 4. (a) The experimental results (points) and theoretical prediction (lines) for the degree of nonseparability of the vector modes in the subspaces $\ell = 1$ and 10 , with increasing turbulence strength. The experimental output VQF with respect to the known input VQF under the effect of turbulence strengths of (b) $D/r_0 = 2.5$ and (c) $D/r_0 = 3.5$. In the absence of perturbations, the output VQF maps onto the diagonal (“No perturbation”) line. The circles are for vector modes in the subspace of $\ell = 1$ and squares are for $\ell = 10$, while the lines are the theoretical prediction based on the isomorphism. The horizontal error bars are smaller than the points. Each data point is obtained from 30 realizations of the same turbulence strength.

from which the behavior of all other vector beams can be inferred.

V. DISCUSSION

Vector beams possess nonseparable coupling between their polarization and spatial components and exhibit correlations similar to entangled pairs of photons. In this paper, we use this fact to study the decay of vector beams in atmospheric turbulence both qualitatively and quantitatively by invoking properties such as channel-state duality [58,59] and the factorization law [57]. These features are unique to quantum entangled states and are commonly used for channel (medium) characterization [72]. Our results confirm that the nonseparability of any other partially ($VQF < 1$) nonseparable vector mode is purely determined by that of a maximally ($VQF \approx 1$) nonseparable vector mode experiencing the same turbulence within the same subspace of optical modes. Interestingly, this does not limit the method for characterization purposes but creates the possibility of using such vector modes as a means to overcome quantum state perturbations; for example, by selecting higher-order modes (e.g., $\ell = 10$ as opposed to $\ell = 1$), or for unscrambling complex

aberrations by using classical light or appropriate high-dimensional quantum states [73]. The extension of the latter to classical beams could be used as an additional tool for adaptive optics, since vector modes can carry information related to the channel and/or medium. While we demonstrate this method for turbulence, it can in principle be extended to various scenarios where optical aberrations are encountered; for example, arising from imperfections or overheating in optical elements in high-power regimes or an optical medium that induces intermodal crosstalk through other mechanisms (e.g., a multimode fiber). In other words, the method is adaptable to any medium that is compatible with the modal scattering mechanism given in Eq. 5. Finally, we point out that the use of the DMD makes the approach very fast, up to kilohertz rates [74], which makes the approach “real-time” for most beam-perturbation processes, such as turbulence, thermal loading, mechanical stress, and so on.

VI. CONCLUSION

In summary, we exploit the concept of channel-state duality analogously to characterize the evolution of various vector or scalar modes through turbulence, demonstrating that the evolution of vector beams can be used to study how various spatial modes decay through turbulence. We show this for two subspaces, $\ell = 1$ and $\ell = 10$, with our results demonstrating that higher-order OAM vector modes decay rapidly while also maintaining a high nonseparability. Our work is integral to the development of alternative methods for characterizing optical beams by borrowing principles from quantum mechanics, with possible applications in various scenarios where complex perturbations are encountered.

TABLE I. An analysis of the different OAM subspace through turbulence. The values in brackets correspond to the theoretical values. Here, the gradients, m_ℓ , correspond to VQF_{\max} .

D/r_0	$\Delta\ell(\ell = 1)$	$\Delta\ell(\ell = 10)$	m_1	R_1^2	m_{10}	R_{10}^2
0	0.05 (0)	0.84 (0)
2.5	3.18 (4.1)	6.64 (9)	0.40	0.97	0.94	0.99
3.5	4.44 (5.59)	8.79 (11.94)	0.21	0.97	0.92	0.98

ACKNOWLEDGEMENT

I.N. acknowledges funding from the Department of Science and Technology (South Africa); S.J. thanks the Department of Science and Technology, Government of India, for funding her visit to WITS through the project DST/IMRCD/BRICS/Pilotcall1/OPTIMODE/2017.

APPENDIX: SCATTERING PROBABILITY OF OAM IN TURBULENCE

The detection probability of an OAM beam propagated through turbulence can be computed from

$$P(l, m) = \iint C_\psi(r, \Delta\theta, z) r dr \times \frac{\exp(-im\Delta\theta)}{2\pi} d\Delta\theta, \quad (\text{A1})$$

where ℓ is the input OAM index of the beam and m is the index for the scattered mode, while $C_\psi(r, \Delta\theta, z)$ is the rotational coherence function defined in cylindrical coordinates, (r, θ, z) , defined as [75]

$$C_\psi(r, \Delta\theta, z) = \langle \psi^*(r, 0, z) \psi(r, \Delta\theta, z) \rangle. \quad (\text{A2})$$

Here, $\psi(r, \theta, z) = u(r, \theta, z) \exp[i\phi(r, \theta)]$ is the beam profile after propagating a distance z with an initial profile of $u(r, \theta, 0)$ at the waist plane and $\exp[i\phi(r, \theta)]$ is the accumulated phase according to the Rytov approximation.

For LG beams, the integral in Eq. (A1) has been solved analytically, yielding the expression [71]

$$P(l, m) = \left(\frac{1}{t}\right)^{|\ell|+1} \left(\frac{t-1}{t+1}\right)^n \sum_{k=0}^{|\ell|} \binom{|\ell|+n}{k} \times \binom{2|\ell|-k}{\ell} \left(\frac{4t}{(t-1)^2}\right)^{k-|\ell|} \quad (\text{A3})$$

where $n = |\ell - m|$, $t = \sqrt{1 + \xi}$ while $\xi = 3.44 \times 2^{2/3} [w_0/(r_0)]^2$, in which w_0 is the waist size of the Gaussian argument in the LG mode and r_0 is the Fried parameter. We rescale the Gaussian argument, i.e., $w_\ell = w_0/\sqrt{|\ell| + 1}$, so that each OAM mode has the same diameter, $D := \sqrt{8}w_\ell$ [33] and experience the same turbulence strength, D/r_0 .

- [4] C. Rosales-Guzmán, B. Ndagano, and A. Forbes, A review of complex vector light fields and their applications, *J. Opt.* **20**, 123001 (2018).
- [5] M. Li, S. Yan, Y. Zhang, Y. Liang, P. Zhang, and B. Yao, Optical sorting of small chiral particles by tightly focused vector beams, *Phys. Rev. A* **99**, 033825 (2019).
- [6] Y. Zhang, B. Ding, and T. Suyama, Trapping two types of particles using a double-ring-shaped radially polarized beam, *Phys. Rev. A* **81**, 023831 (2010).
- [7] N. Bhebhe, P. A. C. Williams, C. Rosales-Guzmán, V. Rodriguez-Fajardo, and A. Forbes, A vector holographic optical trap, *Sci. Rep.* **8**, 1 (2018).
- [8] S. Berg-Johansen, F. Töppel, B. Stiller, P. Banzer, M. Ornigotti, E. Giacobino, G. Leuchs, A. Aiello, and C. Marquardt, Classically entangled optical beams for high-speed kinematic sensing, *Optica* **2**, 864 (2015).
- [9] G. Milione, M. P. J. Lavery, H. Huang, Y. Ren, G. Xie, T. An Nguyen, E. Karimi, L. Marrucci, D. A. Nolan, R. R. Alfano, *et al.*, 4×20 gbit/s mode division multiplexing over free space using vector modes and a q -plate mode (de)multiplexer, *Opt. Lett.* **40**, 1980 (2015).
- [10] Y. Zhao and J. Wang, High-base vector beam encoding/decoding for visible-light communications, *Opt. Lett.* **40**, 4843 (2015).
- [11] A. E. Willner, Vector-mode multiplexing brings an additional approach for capacity growth in optical fibers, *Light: Sci. Appl.* **7**, 18002 (2018).
- [12] M. de Oliveira, I. Nape, J. Pinnell, N. Tabebordbar, and A. Forbes, Experimental high-dimensional quantum secret sharing with spin-orbit-structured photons, *Phys. Rev. A* **101**, 042303 (2020).
- [13] A. Sit, F. Bouchard, R. Fickler, J. Gagnon-Bischoff, H. Larocque, K. Heshami, D. Elser, C. Peuntinger, K. Günthner, B. Heim, *et al.*, High-dimensional intracity quantum cryptography with structured photons, *Optica* **4**, 1006 (2017).
- [14] D. Cozzolino, D. Bacco, B. Da Lio, K. Ingerslev, Y. Ding, K. Dalgaard, P. Kristensen, M. Galili, K. Rottwitt, S. Ramachandran, *et al.*, Orbital Angular Momentum States Enabling Fiber-Based High-Dimensional Quantum Communication, *Phys. Rev. Appl.* **11**, 064058 (2019).
- [15] V. Parigi, V. D'Ambrosio, C. Arnold, L. Marrucci, F. Sciarrino, and J. Laurat, Storage and retrieval of vector beams of light in a multiple-degree-of-freedom quantum memory, *Nat. Commun.* **6**, 1 (2015).
- [16] B. Sun, A. Wang, L. Xu, C. Gu, Z. Lin, H. Ming, and Q. Zhan, Low-threshold single-wavelength all-fiber laser generating cylindrical vector beams using a few-mode fiber Bragg grating, *Opt. Lett.* **37**, 464 (2012).
- [17] D. Naidoo, F. S. Roux, A. Dudley, I. Litvin, B. Piccirillo, L. Marrucci, and A. Forbes, Controlled generation of higher-order Poincaré sphere beams from a laser, *Nat. Photonics* **10**, 327 (2016).
- [18] H. Sroor, Y.-W. Huang, B. Sephton, D. Naidoo, A. Vallés, V. Ginis, C.-W. Qiu, A. Ambrosio, F. Capasso, and A. Forbes, High-purity orbital angular momentum states from a visible metasurface laser, *Nat. Photonics* **14**, 498 (2020).
- [19] L. Marrucci, The q -plate and its future, *J. Nanophotonics* **7**, 078598 (2013).
- [20] R. C. Devlin, A. Ambrosio, N. A. Rubin, J. P. Balthasar Mueller, and F. Capasso, Arbitrary spin-to-orbital

- [1] H. Rubinsztein-Dunlop, A. Forbes, M. V. Berry, M. R. Dennis, D. L. Andrews, M. Mansuripur, C. Denz, C. Alpmann, P. Banzer, T. Bauer, *et al.*, Roadmap on structured light, *J. Opt.* **19**, 013001 (2016).
- [2] Q. Zhan, Cylindrical vector beams: From mathematical concepts to applications, *Adv. Opt. Photonics* **1**, 1 (2009).
- [3] B. Ndagano, I. Nape, M. A. Cox, C. Rosales-Guzman, and A. Forbes, Creation and detection of vector vortex modes for classical and quantum communication, *J. Lightwave Technol.* **36**, 292 (2017).

- angular momentum conversion of light, *Science* **358**, 896 (2017).
- [21] J. P. Balthasar Mueller, N. A. Rubin, R. C. Devlin, B. Groever, and F. Capasso, Metasurface Polarization Optics: Independent Phase Control of Arbitrary Orthogonal States of Polarization, *Phys. Rev. Lett.* **118**, 113901 (2017).
- [22] C. Rosales-Guzmán, X.-B. Hu, A. Selyem, P. Moreno-Acosta, S. Franke-Arnold, R. Ramos-Garcia, and A. Forbes, Polarisation-insensitive generation of complex vector modes from a digital micromirror device, *Sci. Rep.* **10**, 1 (2020).
- [23] E. Nagali, L. Sansoni, L. Marrucci, E. Santamato, and F. Sciarrino, Experimental generation and characterization of single-photon hybrid ququarts based on polarization and orbital angular momentum encoding, *Phys. Rev. A* **81**, 052317 (2010).
- [24] S. Slussarenko, V. D'Ambrosio, B. Piccirillo, L. Marrucci, and E. Santamato, The polarizing Sagnac interferometer: A tool for light orbital angular momentum sorting and spin-orbit photon processing, *Opt. Express* **18**, 27205 (2010).
- [25] G. F. Walsh, Pancharatnam-Berry optical element sorter of full angular momentum eigenstate, *Opt. Express* **24**, 6689 (2016).
- [26] B. Ndagano, I. Nape, B. Perez-Garcia, S. Scholes, R. I. Hernandez-Aranda, T. Konrad, M. P. J. Lavery, and A. Forbes, A deterministic detector for vector vortex states, *Sci. Rep.* **7**, 1 (2017).
- [27] A. Selyem, C. Rosales-Guzmán, S. Croke, A. Forbes, and S. Franke-Arnold, Basis-independent tomography and nonseparability witnesses of pure complex vectorial light fields by Stokes projections, *Phys. Rev. A* **100**, 063842 (2019).
- [28] A. Manthalkar, I. Nape, N. Tabebordbar, C. Rosales-Guzmán, S. Bhattacharya, A. Forbes, and A. Dudley, All-digital Stokes polarimetry with a digital micromirror device, *Opt. Lett.* **45**, 2319 (2020).
- [29] K. Singh, N. Tabebordbar, A. Forbes, and A. Dudley, Digital Stokes polarimetry and its application to structured light: Tutorial, *JOSA A* **37**, C33 (2020).
- [30] M. McLaren, T. Konrad, and A. Forbes, Measuring the nonseparability of vector vortex beams, *Phys. Rev. A* **92**, 023833 (2015).
- [31] B. Ndagano, H. Sroor, M. McLaren, C. Rosales-Guzmán, and A. Forbes, Beam quality measure for vector beams, *Opt. Lett.* **41**, 3407 (2016).
- [32] J. Whinnery, D. Miller, and F. Dabby, Thermal convention and spherical aberration distortion of laser beams in low-loss liquids, *IEEE J. Quantum Electron.* **3**, 382 (1967).
- [33] L. C. Andrews and R. L. Phillips, *Laser Beam Propagation through Random Media* (SPIE, Bellingham, Washington, 2005).
- [34] W. Cheng, J. W. Haus, and Q. Zhan, Propagation of scalar and vector vortex beams through turbulent atmosphere, in *Atmospheric Propagation of Electromagnetic Waves III* Vol. 7200 (International Society for Optics and Photonics, 2009) p. 720004.
- [35] F. Hufnagel, A. Sit, F. Bouchard, Y. Zhang, D. England, K. Heshami, B. J. Sussman, and E. Karimi, Investigation of underwater quantum channels in a 30 meter flume tank using structured photons, *New J. Phys.* **22**, 093074 (2020).
- [36] B. Ndagano, R. Brüning, M. McLaren, M. Duparré, and A. Forbes, Fiber propagation of vector modes, *Opt. Express* **23**, 17330 (2015).
- [37] S. Chen and J. Wang, Theoretical analyses on orbital angular momentum modes in conventional graded-index multimode fibre, *Sci. Rep.* **7**, 1 (2017).
- [38] F. S. Roux, Infinitesimal-propagation equation for decoherence of an orbital-angular-momentum-entangled biphoton state in atmospheric turbulence, *Phys. Rev. A* **83**, 053822 (2011).
- [39] A. Hamadou Ibrahim, F. S. Roux, M. McLaren, T. Konrad, and A. Forbes, Orbital-angular-momentum entanglement in turbulence, *Phys. Rev. A* **88**, 012312 (2013).
- [40] G. A. Tyler and R. W. Boyd, Influence of atmospheric turbulence on the propagation of quantum states of light carrying orbital angular momentum, *Opt. Lett.* **34**, 142 (2009).
- [41] B. J. Smith and M. G. Raymer, Two-photon wave mechanics, *Phys. Rev. A* **74**, 062104 (2006).
- [42] N. Leonhard, G. Sorelli, V. N. Shatokhin, C. Reinlein, and A. Buchleitner, Protecting the entanglement of twisted photons by adaptive optics, *Phys. Rev. A* **97**, 012321 (2018).
- [43] B.-J. Pors, C. H. Monken, E. R. Eliel, and J. P. Woerdman, Transport of orbital-angular-momentum entanglement through a turbulent atmosphere, *Opt. Express* **19**, 6671 (2011).
- [44] M. Malik, M. O'Sullivan, B. Rodenburg, M. Mirhosseini, J. Leach, M. P. J. Lavery, M. J. Padgett, and R. W. Boyd, Influence of atmospheric turbulence on optical communications using orbital angular momentum for encoding, *Opt. Express* **20**, 13195 (2012).
- [45] M. A. Cox, C. Rosales-Guzmán, M. P. J. Lavery, D. J. Versfeld, and A. Forbes, On the resilience of scalar and vector vortex modes in turbulence, *Opt. Express* **24**, 18105 (2016).
- [46] M. Krenn, J. Handsteiner, M. Fink, R. Fickler, and A. Zeilinger, Twisted photon entanglement through turbulent air across Vienna, *Proc. Natl. Acad. Sci.* **112**, 14197 (2015).
- [47] M. Krenn, R. Fickler, M. Fink, J. Handsteiner, M. Malik, T. Scheidl, R. Ursin, and A. Zeilinger, Communication with spatially modulated light through turbulent air across Vienna, *New J. Phys.* **16**, 113028 (2014).
- [48] C. Chen and H. Yang, Characterizing the radial content of orbital-angular-momentum photonic states impaired by weak-to-strong atmospheric turbulence, *Opt. Express* **24**, 19713 (2016).
- [49] B. Ndagano, B. Perez-Garcia, F. S. Roux, M. McLaren, C. Rosales-Guzman, Y. Zhang, O. Mouane, R. I. Hernandez-Aranda, T. Konrad, and A. Forbes, Characterizing quantum channels with non-separable states of classical light, *Nat. Phys.* **13**, 397 (2017).
- [50] A. Aiello, F. Töppel, C. Marquardt, E. Giacobino, and G. Leuchs, Quantum-like nonseparable structures in optical beams, *New J. Phys.* **17**, 043024 (2015).
- [51] F. Töppel, A. Aiello, C. Marquardt, E. Giacobino, and G. Leuchs, Classical entanglement in polarization metrology, *New J. Phys.* **16**, 073019 (2014).
- [52] A. Forbes, A. Aiello, and B. Ndagano, Classically entangled light, in *Progress in Optics* Vol. 64 (Elsevier, 2019) p. 99.

- [53] R. J. C Spreeuw, A classical analogy of entanglement, *Found. Phys.* **28**, 361 (1998).
- [54] J. H. Eberly, X.-F. Qian, A. Al Qasimi, H. Ali, M. A. Alonso, R. Gutiérrez-Cuevas, B. J Little, J. C. Howell, T. Malhotra, and A. N. Vamivakas, Quantum and classical optics—emerging links, *Phys. Scr.* **91**, 063003 (2016).
- [55] T. Konrad and A. Forbes, Quantum mechanics and classical light, *Contemp. Phys.* **60**, 1 (2019).
- [56] E. Toninelli, B. Ndagano, A. Vallés, B. Sephton, I. Nape, A. Ambrosio, F. Capasso, M. J. Padgett, and A. Forbes, Concepts in quantum state tomography and classical implementation with intense light: A tutorial, *Adv. Opt. Photonics* **11**, 67 (2019).
- [57] T. Konrad, F. De Melo, M. Tiersch, C. Kasztelan, A. Aragão, and A. Buchleitner, Evolution equation for quantum entanglement, *Nat. Phys.* **4**, 99 (2008).
- [58] A. Jamiołkowski, Linear transformations which preserve trace and positive semidefiniteness of operators, *Rep. Math. Phys.* **3**, 275 (1972).
- [59] M.-D. Choi, Completely positive linear maps on complex matrices, *Linear Algebra Appl.* **10**, 285 (1975).
- [60] C. Rosales-Guzmán, N. Bhebhe, and A. Forbes, Simultaneous generation of multiple vector beams on a single SLM, *Opt. Express* **25**, 25697 (2017).
- [61] W. K. Wootters, Entanglement of formation and concurrence, *Quantum Inf. Comput.* **1**, 27 (2001).
- [62] H. Sroor, N. Lisa, D. Naidoo, I. Litvin, and A. Forbes, Purity of Vector Vortex Beams through a Birefringent Amplifier, *Phys. Rev. Appl.* **9**, 044010 (2018).
- [63] E. Otte, I. Nape, C. Rosales-Guzmán, A. Vallés, C. Denz, and A. Forbes, Recovery of nonseparability in self-healing vector Bessel beams, *Phys. Rev. A* **98**, 053818 (2018).
- [64] M. A. Cox, N. Mphuthi, I. Nape, N. P. Mashaba, L. Cheng, and A. Forbes, Structured Light in Turbulence, [arXiv:2005.14586](https://arxiv.org/abs/2005.14586) (2020).
- [65] D. L. Fried, Statistics of a geometric representation of wavefront distortion, *JoSA* **55**, 1427 (1965).
- [66] L. Zhang, F. Shen, B. Lan, and A. Tang, Mode-dependent crosstalk and detection probability of orbital angular momentum of optical vortex beam through atmospheric turbulence, *J. Opt.* **22**, 075607 (2020).
- [67] V. Arrizón, U. Ruiz, R. Carrada, and L. A. González, Pixelated phase computer holograms for the accurate encoding of scalar complex fields, *JOSA A* **24**, 3500 (2007).
- [68] S. M. Zhao, J. Leach, L. Y. Gong, J. Ding, and B. Y. Zheng, Aberration corrections for free-space optical communications in atmosphere turbulence using orbital angular momentum states, *Opt. Express* **20**, 452 (2012).
- [69] D. Flamm, D. Naidoo, C. Schulze, A. Forbes, and M. Duparré, Mode analysis with a spatial light modulator as a correlation filter, *Opt. Lett.* **37**, 2478 (2012).
- [70] W.-H. Lee, Binary computer-generated holograms, *Appl. Opt.* **18**, 3661 (1979).
- [71] Y. Zhai, S. Fu, J. Zhang, X. Liu, H. Zhou, and C. Gao, Turbulence aberration correction for vector vortex beams using deep neural networks on experimental data, *Opt. Express* **28**, 7515 (2020).
- [72] M. Malik, H. Shin, M. O'Sullivan, P. Zerom, and R. W. Boyd, Quantum Ghost Image Identification with Correlated Photon Pairs, *Phys. Rev. Lett.* **104**, 163602 (2010).
- [73] N. Herrera Valencia, S. Goel, W. McCutcheon, H. Defenne, and M. Malik, Unscrambling entanglement through a complex medium, *Nat. Phys.* **16**, 1 (2020).
- [74] S. Scholes, R. Kara, J. Pinnell, V. Rodríguez-Fajardo, and A. Forbes, Structured light with digital micromirror devices: A guide to best practice, *Opt. Eng.* **59**, 041202 (2019).
- [75] C. Paterson, Atmospheric Turbulence and Orbital Angular Momentum of Single Photons for Optical Communication, *Phys. Rev. Lett.* **94**, 153901 (2005).